Radio Science

RESEARCH ARTICLE
10.1029/2021RS007420

Ionospheric Scintillation Monitoring With ROTI From Geodetic Receiver: Limitations and Performance Evaluation

Wei Li[1,2], **Shuli Song**[1], **and Xulei Jin**[1,2]

[1]Shanghai Astronomical Observatory, Chinese Academy of Sciences, Shanghai, China, [2]University of Chinese Academy of Sciences, Beijing, China

Key Points:

- Limitations of Rate of change of Total electron content Index (ROTI) in indicating the occurrence of ionospheric scintillation are summarized and performance is quantitatively evaluated for the first time
- The integrity of ROTI derived from different sampling rates data is compared. A reasonable threshold of 0.25 m for cycle slip detection of 30s sampling interval data is proposed
- Reliability of ROTI obtained from different sampling rates data in response to ionospheric scintillation is presented. Correlation is compared

Correspondence to:
S. Song,
slsong@shao.ac.cn

Citation:
Li, W., Song, S., & Jin, X. (2022). Ionospheric scintillation monitoring with ROTI from geodetic receiver: Limitations and performance evaluation. *Radio Science*, *57*, e2021RS007420. https://doi.org/10.1029/2021RS007420

Received 22 DEC 2021
Accepted 6 MAY 2022

Abstract By comparing amplitude scintillation index S_4 from scintillation receivers and Rate of change of Total electron content Index (ROTI) from nearby geodetic receivers in low latitude region of China during year 2015, this work summarized the limitations of ROTI in indicating ionospheric scintillation and quantitatively evaluated the performance/reliability of ROTI in monitoring ionospheric scintillation in low latitude region. The results indicate that the correlation between ROTI and S_4 is lower (higher) when scintillation occurs at lower (higher) satellite elevation angle. Erroneous cycle slips and longer ROTI calculation time interval degrade the integrity of ROTI calculated from 30-s sampling interval data (abbreviated as 30s-ROTI). ROTI calculated from 1-s sampling interval data (abbreviated as 1s-ROTI) has better integrity (90%) than that of 30s-ROTI (60%). In addition, we propose a reasonable threshold of 0.25 m for cycle slip detection for the 30-s cadence observation data to avoid misjudging a large ionospheric variation as a cycle slip and further improve on the integrity of 30s-ROTI. The deviation of ROTI from S_4 decreases the reliability of ROTI in indicating the occurrence of ionospheric scintillation as well as the correlation between ROTI and S_4. The reliability of ROTI in indicating the occurrence of scintillation can reach 80% and 88% for 30s ROTI and 1s-ROTI, respectively. The deviation causes 60% of the correlations between 30s-ROTI and S_4 drop by 0.15 ~ 0.2 and causes more than 66% of the correlations between 1s-ROTI and S_4 drop by 0.15 ~ 0.2. These results establish an important reference concerning the reliability of ROTI in indicating the occurrence of ionospheric scintillation.

Plain Language Summary The correlation between Rate of change of Total electron content Index (ROTI) and S_4 is dependent on the satellite elevation angle where scintillation occurs. The integrity of ROTI derived from low sampling rate data is lower than that of ROTI derived from high sampling rate data by about 30% due to erroneous cycle slips and longer ROTI calculation time interval. A reasonable threshold of 0.25 m for cycle slip detection is proposed to avoid the erroneous cycle slips on low sampling rate data. The reliability of ROTI obtained from low and high sampling rate data in response to ionospheric scintillation may be as high as 80% and 88%, respectively.

1. Introduction

During the period from sunset to midnight on equinox months, deep and frequent fading of radio signals is observed due to the ionospheric irregularities within plasma bubbles in the ionosphere when the signals pass through this region (Aarons et al., 1975). Satellite communications at equatorial latitudes are found not to be as reliable as have been originally expected (Woodman & Hoz, 1976). This kind of phenomenon on radio signals is referred to as ionospheric scintillation. Ionospheric scintillation has an adverse effect on the quality of Global Navigation Satellite System (GNSS) observation data and can further degrade the performance of its application. Many studies suggest that ionospheric scintillation may cause frequent cycle slips and loss of signal lock of Global Navigation Satellite System (GNSS) observation data. For example, Thomas et al. (2001) pointed out that when the amplitude scintillation index, S_4, >0.6, up to 45% of satellite-receiver links are affected. Conker et al. (2003) derived the relationship between ionospheric scintillation indices and tracking loop error of GPS measurements and pointed out that the phase tracking errors that exceed the 10-degrees threshold or the amplitude scintillation of L1 that exceed 0.707 will result in loss of lock. Humphreys, Psiaki and Kintner et al. (2010) and Humphreys, Psiaki, Ledvina, et al. (2010) pointed out that cycle slips are often associated with deep power fades (>15 dB) of GPS frequencies. Xiong et al. (2016) studied the loss of lock of spaceborne receivers and pointed out that at low latitude region, the Swarm satellite's loss of total GPS signals is related to the depletion depths of electron density larger than $10 \times 10^{11} \mathrm{m}^{-1}$. Yang et al. (2020) investigated the performance of precise point positioning solutions and results show significantly increased positioning error during ionospheric scintillation. For these reasons,

scintillation has become one of the major concerns in Global Navigation Satellite System (GNSS) applications. Therefore, monitoring and studying ionospheric scintillation is of significant interest for the correction and/or mitigation of the effects of scintillation on GNSS positioning and navigation.

A number of ionospheric scintillation monitoring (ISM) receivers have been installed in the regions with frequent scintillations, for example, equatorial and high latitude regions, to monitor and study ionospheric scintillation. In practice, the ionospheric scintillation monitoring (ISM) receivers are located in a very limited number of monitoring stations. Furthermore, they are designed to sample data at high frequency (normally 50 Hz) to capture the scintillation information and thus data at such a sampling rate requires substantial memory to store and robust communication capabilities to transfer. As a consequence, observation data from ionospheric scintillation monitoring (ISM) receivers are not typically openly available which hinders the data sharing among researchers and joint study ionospheric scintillation. Pi et al. (1997) proposed the Rate of change of total electron content (TEC) index (ROTI) to measure ionospheric irregularities. The main advantage of ROTI over scintillation indices is that it is calculated from dual-frequency phase observation of common geodetic receivers, which are more widely distributed in the world than ISM receivers. The worldwidely distributed and openly accessible GPS/GNSS stations make it feasible to use ROTI to observe ionospheric irregularities/scintillations in a large or global region. Several studies have investigated the correlation between ROTI and S_4 and the ratio of ROTI/S_4 to prove the consistency of ROTI with S_4, for example, (Basu et al., 1999; Carrano et al., 2019; Li et al., 2007; Pi et al., 2013; Xu et al., 2007; Yang & Liu, 2015). Basu et al. (1999) pointed out that the ratio of ROTI/S_4 varied between 2 and 10 at Ascension Island (7.93°S, 14.42°W). Li et al. (2007) found that the ratio of ROTI/S_4 varied between 0.3 and 6 at Sanya, China (18.33°N, 109.52°E). Xu et al. (2007) showed that the ROTI and S_4 have a remarkable positive correlation and the correlation value can reach 0.97 at maximum. Pi et al. (2013) found that ROTI and L1 phase scintillation index, σ_φ, were well correlated and the correlation coefficient reached 0.763. Yang and Liu (2015) analyzed the correlation between ROTI and S_4/σ_φ and pointed out that the correlation coefficient between ROTI and S_4/σ_φ is about 0.6 with all GPS satellites being used together and reaches 0.8 with each individual satellite being considered. Carrano et al. (2019) further showed that the correlation between ROTI and S_4 depends on the effective scan velocity between the ionospheric penetration point and the drifting irregularities and that the ratioROTI/S_4 depends on the line-of-sight angle with respect to the the magnetic field line. Jacobsen (2014) analyzed the impact of different sampling rates and calculation time intervals on ROTI values and found that a lower sample rate lowered the ROTI value and that a longer calculation time interval removed or reduced short-lived peaks of ROTI.

The International GNSS Service has provided GNSS users ROTI map products based on the observation data of 30-s sampling interval from about 700 GNSS stations over the northern hemisphere since 2014 for retrospective estimation of space weather impact on positioning (Cherniak, Krankowski, & Zakharenkova, 2014; Cherniak, Zakharenkova, & Krankowski, 2014). Based on the ROTI map, several studies have been carried out to investigate the characteristics of ionospheric irregularities induced by geomagnetic storm and the relationship between ionospheric irregularities and other space weather, for example, auroral activity, large-scale traveling ionospheric disturbances, equatorial plasma bubbles enhancement (Cherniak et al., 2018; Cherniak & Zakharenkova, 2015; Zakharenkova et al., 2016, 2019). Mrak et al. (2020) use 1-s data from geodetic receiver to construct proxy phase and amplitude scintillation indices and validate them against ROTI and S_4. In fact, ROTI calculated from different strategies has different performance in manifesting ionospheric scintillation. The tough challenge of correctly detecting and repairing cycle slips of low sampling rate observation (e.g., 30 s) may inevitably influence the performance of ROTI. In addition, the temporal/spatial scale size of ionospheric irregularities measured by ROTI is different from that measured by scintillation indices (Basu et al., 1978), which may also reduce the reliability of ROTI in indicating the presence of ionospheric scintillation. For GNSS users, the more concerned is not ionospheric irregularities but ionospheric scintillation since the latter degrades the performance of GNSS applications. Given that the limited distribution of ISM receivers could not provide a global/regional measure of ionospheric scintillation over the world, ROTI may be achievable as an alternative indicator to measure global/regional ionospheric irregularities which are associated with scintillation. However, GNSS users lack of a reliable reference concerning the reliability of ROTI in expressing/monitoring ionospheric scintillation. Thus, it is quite necessary to analyze the limitations of ROTI in monitoring ionospheric irregularities that could perhaps cause scintillation and to see to what extent that ROTI is reliable to indicate the occurrence of ionospheric scintillation, for which this study is carried out.

Table 1
Information of Receivers

Station name	Geographical coordinates	Geomagnetic coordinates	Type
HISY	18.28°N, 109.58°E	8.98°N, 177.81°W	ISM
HISY	18.24°N, 109.53°E	8.94°N, 177.86°W	Geodetic
GDSZ	22.38°N, 113.89°E	12.89°N, 173.77°W	ISM
HKTK	22.55°N, 114.22°E	13.30°N, 173.91°W	Geodetic

The study is structured as follows. Section 2 describes the data set and methodology that is used in this study. Section 3 consists of two subsections: Subsection 3.1 presents the general variation of ROTI and S_4 as well as their difference; Subsection 3.2 analyzed the limitations of ROTI in monitoring ionospheric irregularities and associated scintillation and evaluated the performance of ROTI in monitoring ionospheric irregularities and scintillation. Finally, in Section 4, the main conclusions of this work are highlighted and summarized.

2. Data and Methodology

2.1. Data

In this paper, data from an ISM receiver located in Sanya, China (HISY) and an Ionospheric GPS-TEC Scintillation Monitoring (ISM) receiver from Meridian Project located in Shenzhen, China (GDSZ) in 2015 are used to calculate ionospheric scintillation indices. GPS observation data observed by geodetic receivers located in Sanya station (HISY) and Sha Tau Kok station in Hong Kong (HKTK) of both 1-s and 30-s sampling interval are used to calculate ROTI. Data from those days that experience ionospheric scintillation/irregularities (mainly in the equinox months) are used for this study. Table 1 lists some basic information about these four receivers. Since the distances from the geodetic receivers to the ISM receivers are very close, it is practicable to compare ROTI calculated from these two geodetic receivers with ionospheric scintillation indices calculated from the corresponding ISM receivers to compare ROTI and S_4/σ_φ as well as evaluate the performance of ISM with geodetic receivers.

2.2. Methodology

Amplitude scintillation index and phase scintillation index are the most representative indices in expressing ionospheric scintillation. Amplitude scintillation index S_4 can be calculated as below:

$$S_4 = \sqrt{\frac{\langle I^2 \rangle - \langle I \rangle^2}{\langle I \rangle^2}} \tag{1}$$

where I is the detrended signal intensity; $\langle \bullet \rangle$ is an averaging operator over a certain time interval (normally 1 min). Phase scintillation index σ_φ is defined as the standard deviation of detrended carrier phase within 1 min which can be written as

$$\sigma_\varphi = \sqrt{\langle \phi^2 \rangle - \langle \phi \rangle^2} \tag{2}$$

where ϕ is the detrended carrier phase in radians units.

ROTI can be derived from dual-frequency GPS/GNSS phase observations which are obtained as below:

$$\lambda_1 L_1 = \rho + \lambda_1 N_1 + c\delta_r - c\delta^s - I + T - d_1 + \epsilon \tag{3}$$

$$\lambda_2 L_2 = \rho + \lambda_2 N_2 + c\delta_r - c\delta^s - \gamma I + T - d_2 + \epsilon \tag{4}$$

where λ_1 and λ_2 are wavelengths at the frequency f_1 and f_2, respectively; L_1 and L_2 are the carrier phase measurements of two frequencies; ρ is the geometric distance between receiver and satellite; N_1 and N_2 are the integer carrier phase ambiguities of two frequencies; c is the light speed; δ_r and δ^s are the receiver and satellite clock bias, respectively; I is the ionospheric delay on frequency f_1; $\gamma = {f_1}^2/{f_2}^2$ is the frequency factor; T is the tropospheric delay; d_1 and d_2 are the receiver and satellite hardware phase delays at two frequencies; ϵ represents unmodeled error comprising multipath and receiver noise.

Geometry-free (GF) combination of carrier phase L_1 and L_2 can be written as:

$$L_{GF} = L_1\lambda_1 - L_2\lambda_2 = \lambda_1 N_1 - \lambda_2 N_2 + (\gamma - 1)I + d_2 - d_1 \quad (5)$$

As shown in Equation 5, geometry distance, receiver and satellite clock and tropospheric delay are eliminated in the geometry-free combination. By differencing L_{GF} at epoch (i) and epoch (i−1),

$$\Delta L_{GF}(i) = L_{GF}(i) - L_{GF}(i-1) = \lambda_1 \Delta N_1 - \lambda_2 \Delta N_2 + (\gamma - 1)[I(i) - I(i-1)] \quad (6)$$

where $\Delta N_1 = N_1(i)$–$N_1(i$−1) and $\Delta N_2 = N_2(i)$–$N_2(i$−1) are the difference of inter-epoch ambiguity. It should be noted that when no cycle slip occurs, ΔN_1 and ΔN_2 are equal to zero and there is only inter-epoch ionospheric residual (or variation of ionospheric delay) on the right side of the equal sign in Equation 6. It is worth mentioning that ionospheric residual method (represented by Equation 6) and Melbourn-Wubbena (MW) combination method is widely used to detect cycle slip. The M-W combination is given by

$$L_{MW} = \frac{1}{f_1 - f_2}(f_1 L_1 - f_2 L_2) - \frac{1}{f_1 + f_2}(f_1 P_1 + f_2 P_2) \quad (7)$$

where P_1 and P_2 are pseudo-ranges of frequency f_1 and f_2. In this study, we use the inter-epoch difference of geometry-free (GF) combination and Melbourn-Wubbena (MW) combination method (mentioned above) to detect cycle slips. In order to avoid the influence of inaccurate cycle slip repair on the calculation of ROTI, cycle slip detected in the observation data is identified and skipped in the calculation.

ROT is the rate of change of TEC in unit of TECU/minute along the signal propagation path and can be converted from inter epoch ionospheric residual as follows

$$\mathrm{ROT}(i) = \frac{{f_1}^2 \times {f_2}^2}{\Delta t \times 10^{16} \times 40.3 \times \left(f_1^2 - f_2^2\right)} \Delta L_{GF}(i) \quad (8)$$

ROTI is defined as the standard deviation of ROT within a certain period (normally 5 min for observation data of 30-s sampling interval, abbreviated as 30s-5 min ROTI; and 1 min for observation data of 1-s sampling interval, abbreviated as 1s-1 min ROTI). For the purpose of making full use of observation data, ROTI is calculated epoch by epoch with the sliding window moving forward one epoch each time. The algorithm for calculating ROTI is as follows (Pi et al., 1997)

$$\mathrm{ROTI} = \sqrt{\left\langle ROT^2 \right\rangle - \left\langle ROT \right\rangle^2} \quad (9)$$

3. Results and Analysis

3.1. Scintillation Indices, ROTI and Their Difference

The scintillation indices from the ISM receiver and 30s-5 min ROTI from the geodetic receiver at HISY in 2015 are plotted in Figure 1. The same indices for GDSZ (HKTK) are plotted in Figure 2. The omitted series points along the data axis in both Figures 1 and 2 is due to the fact that the days which didn't encounter scintillation are not shown in both figures for the purpose of highlighting the days which encountered scintillation. The data of days that encounter ionospheric scintillation/irregularities is used for the subsequent analysis and evaluation. Due to some days (during February and March) stoppage of ISM receiver at HISY, the number of days encountering scintillation at HISY is less than that at GDSZ. As can be seen from Figures 1 and 2, the ionospheric scintillation occurs mostly in equinox months and that occurs on spring more than on autumn, which is consistent with previous studies (Lee et al., 2005; Tanna et al., 2013). The average number of visible satellites that experience scintillation among these scintillation days are 5.9 and 5.6 at HISY and HKTK station, respectively. The protuberance parts in the sequence of scintillation indices indicate the occurrence of ionospheric scintillation, and 30s-5 min ROTI corresponds to scintillation indices well in general.

Normally, $S_4 > 0.2$ indicates nonnegligible scintillation activity (Muella et al., 2008). ROTI > 0.5 TECu/min indicates the presence of ionospheric irregularities at scale length of a few kilometers (Ma & Maruyama, 2006). For 1s-1 min ROTI, we take 2.5 TECu/min as the critical/threshold value of scintillation (Wei et al., 2019). According to the amount of each scintillation index that exceeds its own critical value of scintillation, Figure 3 presents the hourly average duration of ionospheric scintillation monitored by S_4, 30s-5 min ROTI and 1s-1 min

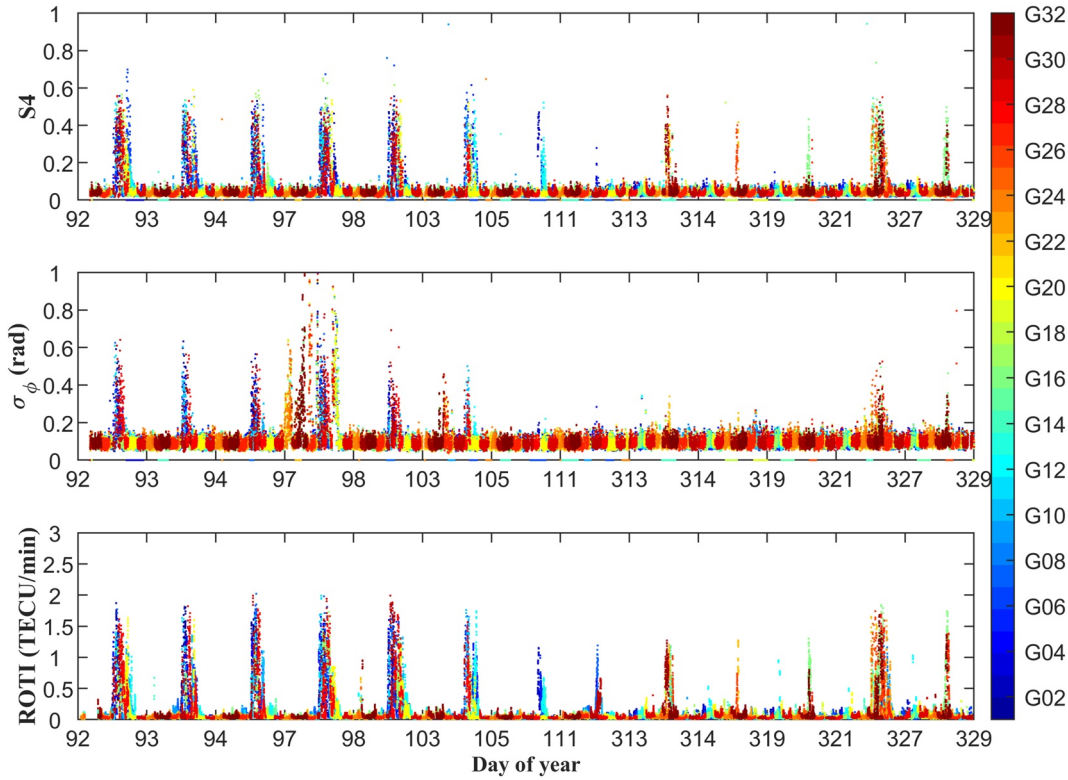

Figure 1. Amplitude scintillation index (top), phase scintillation index (middle) and Rate of change of Total electron content Index (bottom) at HISY station in 2015.

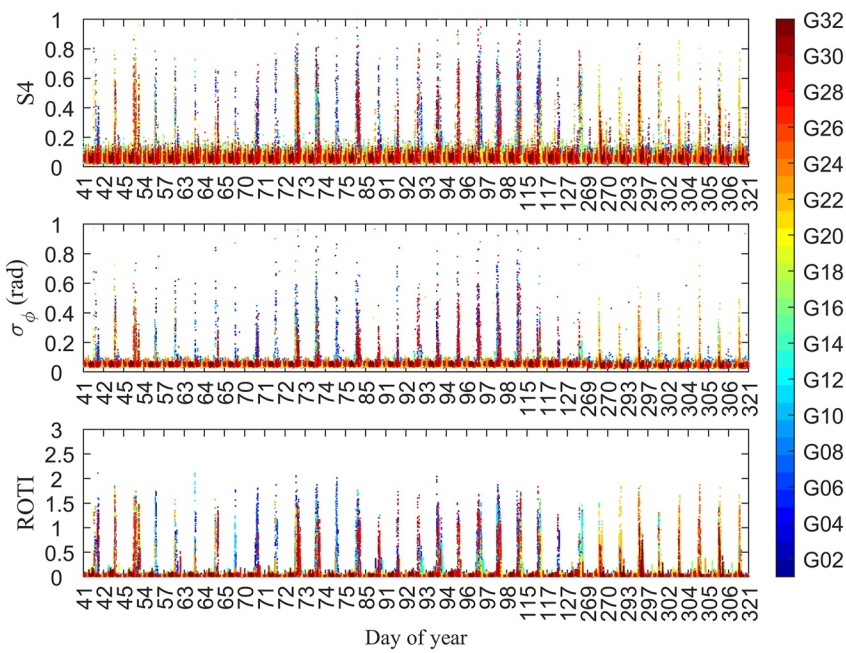

Figure 2. Amplitude scintillation index (top) and phase scintillation index (middle) at GDSZ station and Rate of change of Total electron content Index (bottom) at HKTK station in 2015.

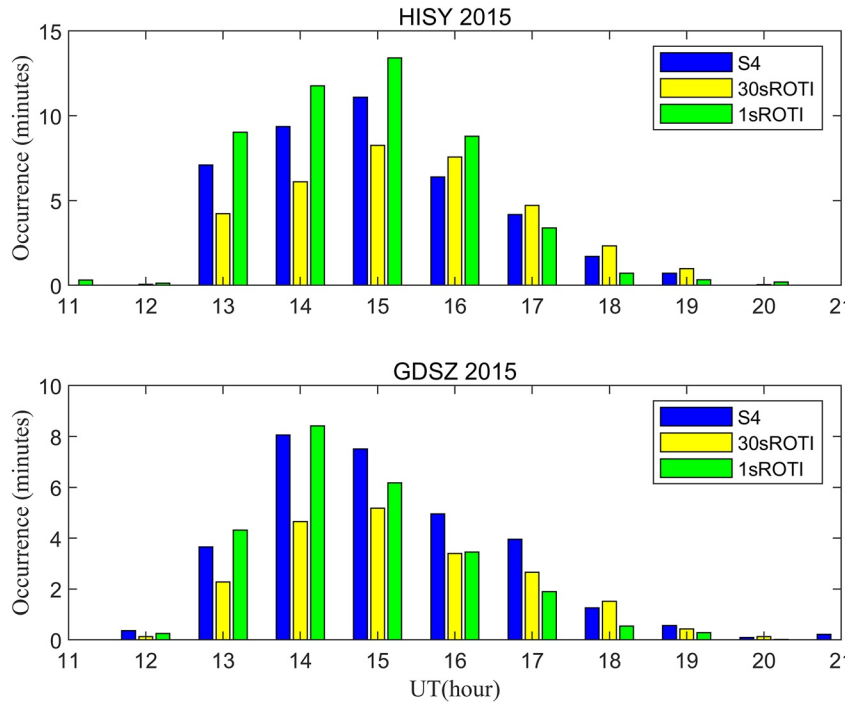

Figure 3. Hourly average duration of scintillation monitored by S_4, 30s-5 min Rate of change of Total electron content Index (ROTI) and 1s-1 min ROTI at HISY (top panel) and GDSZ (bottom panel) in 2015.

ROTI from 11 UT (19 LT) to 21 UT (05 LT) in 2015 at HISY and GDSZ station, respectively. The other periods are not presented in the figure due that no scintillation occurs during those periods. It can be seen from the figure that scintillation began at around 12 UT (20 LT), peaked at around 14–15 UT (22–23 LT), and ended at around 20 UT (04 LT). In addition, there are some differences between the hourly average duration of ionospheric scintillation monitored by S_4 and 30s-5 min ROTI as well as 1s-1 min ROTI. The deviation duration between S_4 and 30s-5 min ROTI as well as 1s-1 min ROTI in Figure 3 may attribute to multiple factors to be discussed in the subsequent sessions.

3.2. Limitations and Performance Evaluation of ROTI

3.2.1. Elevation Angle Dependence

Yang and Liu (2015) analyzed the relationship between maximum elevation angle and correlation among ROTI and scintillation indices and pointed out that satellites with lower maximum elevation angles have smaller correlation coefficients. Since ROTI and S_4/σ_φ have good correlation only when a satellite encounters ionospheric scintillation. Thus, there might exist a freedom between maximum elevation angle and the elevation angle where satellite encounters ionospheric scintillation, for example, satellite A has a maximum elevation angle of 80° and encounters scintillation at elevation of 30° ~ 40° while satellite B has a maximum elevation angle of 70° but encounters scintillation at elevation of 50° ~ 60°, which may distort the conclusion. Instead, we exclusively take the elevation angle where a satellite encounters ionospheric scintillation and to compare its relationship with correlation coefficient between ROTI and S_4/σ_φ. Normally, a satellite is considered to have encountered ionospheric scintillation when its S_4 is greater than 0.2 and lasts for more than 10 min. For those satellites that encounter ionospheric scintillation, the elevation angle is extracted according to the start and end time of scintillation and is averaged as an independent variable, the correlations between ROTI and S_4/σ_φ with the same average-elevation of occurrence of scintillation are averaged as the dependent variable. The statistics are carried out among all GPS satellites which encounter ionospheric scintillation in 2015 at HKTK station and the result is presented in Figure 4.

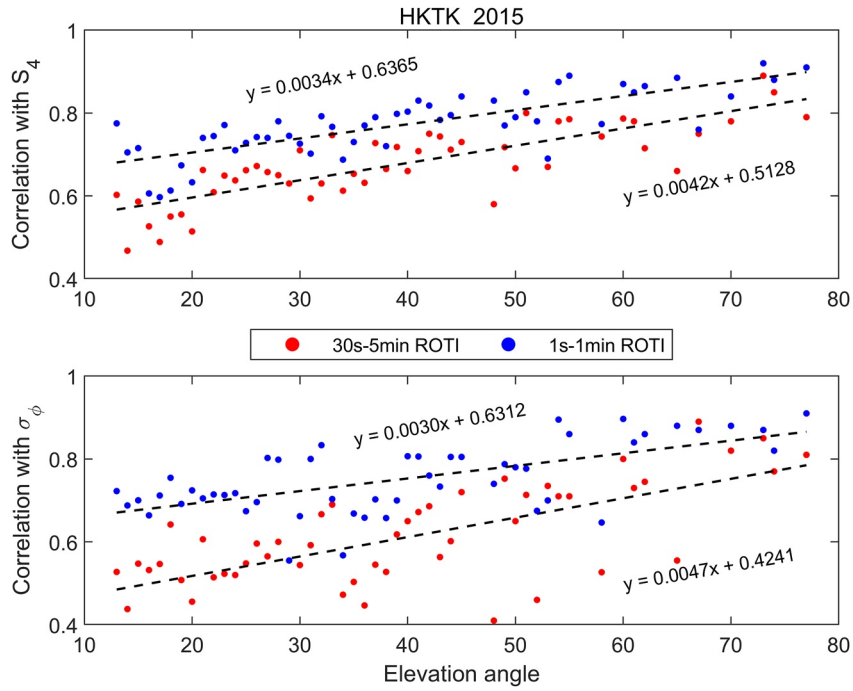

Figure 4. Mean correlation coefficients between Rate of change of Total electron content Index (ROTI) and S_4 (top panel), ROTI and σ_φ (bottom panel) at mean elevation angle where satellites encounter ionospheric scintillation at HKTK station in 2015 (the red and blue scatter represent correlation between 30s and 5 min ROTI and S_4/σ_φ, 1s-1 min ROTI and S_4/σ_φ, respectively).

The red and blue scatter in Figure 4 represent the correlation between 30s and 5 min ROTI and S_4/σ_φ, the correlation between 1s and 1 min ROTI and S_4/σ_φ, respectively. The black dotted line in the figure represents the fitting result of the correlation and the elevation angle. Their fitting relationship is also shown in figure. As revealed by the figure, the correlation between ROTI and S_4/σ_φ increases linearly with the increase of the mean elevation angle where the scintillation occurs. A new discovery is that the increase of the correlation continues until the maximum elevation angle, which implies that a cutoff elevation angle could not completely eliminate the influence of elevation on the deviation between ROTI and scintillation indices. It can also be seen that the correlation between 1s and 1 min ROTI and S_4/σ_φ is higher than that between 30s-5 min ROTI and S_4/σ_φ. The reason that the correlation between ROTI and σ_φ fluctuates larger than that between ROTI and S_4 might be due to that the occurrence of phase scintillation is not as frequent as that of amplitude scintillation in equatorial regions (Doherty et al., 2003). From the overall trend in the figure, the correlation between ROTI and S_4/σ_φ shows dependence on satellite elevation angle, indicating that ROTI has a better consistency with scintillation indices at higher satellite elevation angle. The elevation angle-dependence of correlation between ROTI and scintillation indices is likely related with propagation geometry, which is discussed and confirmed in Carrano et al. (2019) and Yang and Morton (2020). Thus, ROTI may have a weak consistency with scintillation indices when the satellite encounters ionospheric scintillation at a low elevation angle. In the subsequent analysis, a 30° elevation angle mask is adopted to mitigate the influence of elevation angle on the results.

3.2.2. Frequent Cycle Slips and Integrity of ROTI

Ionospheric scintillation causes frequent cycle slips in the carrier phase of GPS observations (Chen et al., 2008; Pi et al., 2017; Prikryl et al., 2010; Zhang et al., 2010). In addition, a large ionospheric variation that exceeds the threshold of cycle slip detection will inevitably lead to misjudging ionospheric variation as cycle slip in the processing of GPS/GNSS data. Here we refer to this kind of a cycle slip as an erroneous cycle slip. Cycle slip mixed in the carrier phase observations, if not properly processed, will cause outliers in ROTI eventually. For observation data of high sampling rate (e.g., 1 s), benefiting from negligible variation of ionosphere within the short time, the cycle slip detection and repairing algorithm should work well (Cai et al., 2013; Liu, 2011). For observation data of low sampling rate (e.g., the 30 s), however, cycle slip may not be detected and repaired

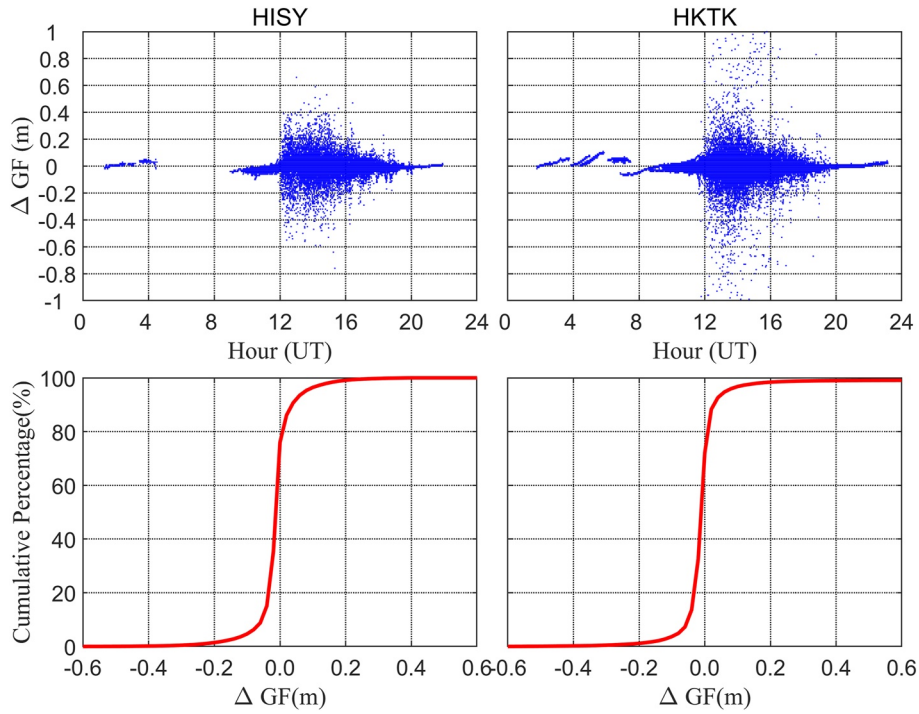

Figure 5. Scatter (top panel) and cumulative histogram (bottom panel) of 30s-ΔGF at HISY (left column) and HKTK (right column) station in 2015 when 1s-ΔGF not appear cycle slip during ionospheric scintillation.

correctly during the ionospheric disturbance period. Thus, data identified with cycle slip is commonly marked and skipped during the processing of GPS/GNSS observation. It should be mentioned that to mitigate the interruption of identified cycle slip to the continuity of ROTI, in our strategy, a ROTI is calculated as long as the number of ROT within the calculation time interval is above 80% of the full length of the calculation time interval, for example, a 30s-5 min ROTI is determined as long as 8 ROTs are available within the 5-min calculation time interval in our calculation. Yet this mitigation strategy plays a little role when frequent cycle slips occur during ionospheric scintillation. As a result, the continuous monitoring ability of ROTI for ionospheric scintillation is still constrained by cycle slips. As shown by Equation 6, since the ionospheric term in the right side of the second equal sign is negligible in a short time (e.g., 1 s), for a small cycle slip pair (1 cycle on L_1 and 1 cycle on L_2), the absolute value of ΔL_{GF} equals $|\lambda_1 - \lambda_2| = 5.4$ cm for GPS observation. Thus, 0.05 m is reasonable to be the threshold of cycle slip detection with the GF method for observation data of 1-s sampling interval (Chen et al., 2016; Zhang et al., 2014). Based on this threshold, the upper limit of ROT derived from 1-s data could reach 28.5TECu/min according to Equation 8. Considering the non-negligible variation of ionosphere within 30 s, Zhang et al. (2017) proposed 0.15 m as the threshold of cycle slip detection with the GF method for GPS observation data of 30-s sampling interval. However, based on Zhang et al. (2017)'s threshold, the upper limit of ROT monitored by 30-s data could only reach 2.85 TECu/min, which is smaller than the ionospheric variation in our actual test. Thus, the threshold proposed by Zhang et al. (2017) is subject to over-constraining.

We use a novel strategy to determine the range of ionospheric variation within 30 s and meanwhile verify the constraint of the threshold 0.15 m during ionospheric scintillation. We chose all satellites that encounter ionospheric scintillation and extract the value of the differential of GF combination between continuous epoch of 30-s sampling interval data (abbreviated as 30s-ΔGF) when no cycle slip appears on the 1-s sampling interval data at the same time according to its differential of GF combination between continuous epoch (abbreviated as 1s-ΔGF). The scatter and cumulative histogram of the extracted 30s-ΔGF is presented in Figure 5. As revealed by Figure 5, the absolute value of a few points of 30s-ΔGF exceeds 0.4 m at HISY and even exceeds 0.6 m at HKTK, which implies that the ionospheric variation within 30 s would exceeds 7.6 TECu/min according to Equation 8. Therefore, it can be inferred that there is not a strict boundary between small cycle slip and large ionospheric variation. The cumulative histograms in the bottom panel of the figure suggest that the value of the majority (98.7%

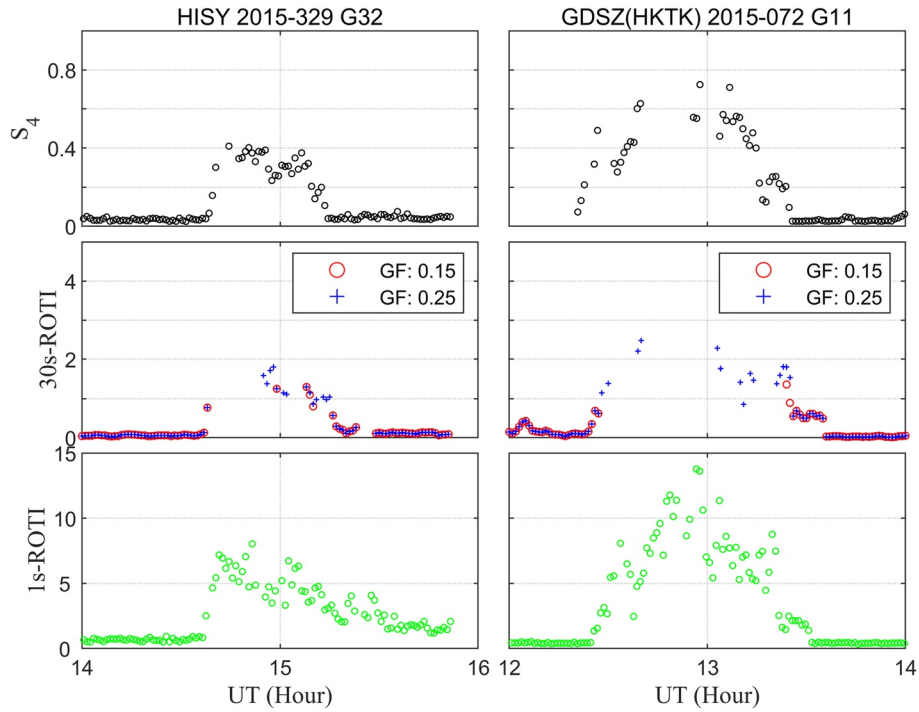

Figure 6. Time series of S_4 (top panel), 30s-5 min Rate of change of Total electron content Index (ROTI) (middle panel) and 1s-1 min ROTI (bottom panel) for satellite G32 at HISY on DOY 329 in 2015 (left column), satellite G11 at GDSZ on DOY 072 in 2015 (right column).

at HISy and 97.9% at HKTK) of 30s-ΔGF is between $-0.25 \sim 0.25$ m. Thus, the threshold 0.15 m is proven to be constrained for cycle slip detection of 30-s sampling interval observation data during ionospheric scintillation.

In this paper, we propose to have 0.25 m as a relatively loose threshold of cycle slip detection with the GF method for 30 s sampling interval data. Note that though 4.76 TECu/min corresponds to the threshold of 0.25 m for 30-s sampling interval data is still smaller than 28.5TECu/min yet it is enough to represent most of the ionospheric variation. In addition, the threshold of 0.15 m is also used in the calculation of ROTI for a comparison. Two worse cases were chosen from HISY and GDSZ respectively to present the impact of troublesome cycle slip on ROTI calculated from low sampling interval (30 s) data. The details are shown in Figure 6. The S_4, 30s-5 min ROTI (determined by two thresholds of GF method) and 1s-1 min ROTI are presented in the top, middle, and bottom of the figure for satellite G32 at HISY on DOY (day of the year) 329 in 2015 (left column) and satellite G11 at GDSZ (HKTK) on DOY 72 in 2015 (right column), respectively. It should be mentioned that both 30s-5 min ROTI and 1s-1 min ROTI in the figure are resampled at an interval of 1 min for a more intuitive comparison with S_4. As shown by Figure 6, the protruding parts in the series of S_4 indicate the occurrence of significant ionospheric scintillation. Correspondingly, the protruding parts in the middle and bottom panel represent ionospheric scintillation monitored by 30s-5 min ROTI and 1s-1 min ROTI, respectively. However, compared with the series of 1s-1 min ROTI, the empty areas in the protruding parts of 30s-5 min ROTI determined by both 0.15 and 0.25 m threshold of cycle slip detection cannot be ignored in the middle panel of the figure. As shown in the middle panel of the figure, the 30s-5 min ROTI determined by 0.25 m threshold has more points than that determined by 0.15 m threshold during ionospheric scintillation, indicating that the large ionospheric variations are misjudged as cycle slips and excluded from the calculation of ROTI by the threshold 0.15 m. In addition, the points of the 30s-5 min ROTI determined by 0.25 m threshold are still less than that of 1s-1 min ROTI indicating that ROTI determined in the 5-min calculation time interval is more likely to be interrupted by cycle slips than that determined by the 1-min calculation time interval.

To further quantify the impact of frequent cycle slips on the performance of ROTI, the integrity of S_4 and ROTI calculated from different strategies during scintillation period is compared. Here, integrity is defined as the ratio of the number of calculated ROTI to the number of expected ROTI, where the expected number of ROTI is

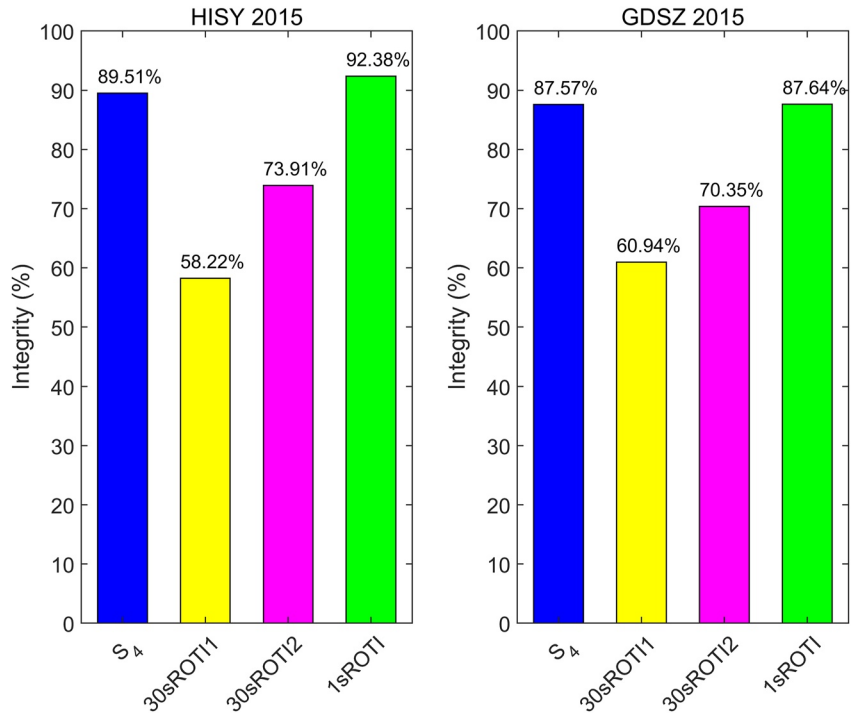

Figure 7. Statistics of integrity of S_4, 30s-5 min Rate of change of Total electron content Index (ROTI) and 1s-1 min ROTI during ionospheric scintillation at HISY station and GDSZ station in 2015.

determined by the number of epochs between the start and the end time of scintillation. It should be mentioned that to focus on the impact of frequent cycle slips on ROTI, only the data of satellites in the period of ionospheric scintillation are counted. The statistic of the integrity of S_4 and ROTI during ionospheric scintillation is shown in Figure 7. The label "30sROTI1" and "30sROTI2" in the figure represent 30s-5 min ROTI determined by 0.15 and 0.25 m threshold, respectively. As shown by Figure 7, the integrity of 1s-1 min ROTI could reach around 90% which is equivalent with that of S_4. However, the integrity of 30s-5 min ROTI determined by 0.15 m threshold could only reach around 60% which is far less than that of 1s-1 min ROTI and S_4. The integrity of 30s-5 min ROTI determined by 0.25 m threshold is about 70%, suggesting that a reasonable threshold of cycle slip detection could improve the integrity of 30s-5 min ROTI by 10% $\sim$ 15% through avoiding judging large ionospheric variation as cycle slip in the calculation of ROTI with 30-s sampling observation data. The integrity of 30s-5 min ROTI determined by 0.25 m threshold is still 18% less than that of 1s-1 min ROTI, indicating that the integrity of ROTI calculated with 5-min time interval is more vulnerable than that calculated with 1-min time interval in case of frequent cycle slip or loss of signal lock.

3.2.3. Deviation of ROTI From S_4

Amplitude scintillations at L band are mainly caused by ionospheric irregularities in the vicinity of Fresnel scale, which can be written as $r_F = \sqrt{2\lambda z}$, where r_F is the scale length of irregularities, λ is the wavelength of the signal, z is the slant range from receiver to the ionospheric piercing point (Beach & Kintner, 1999). For GPS L_1 observation, assuming $z = 400$ km, then the Fresnel dimension is 390m. However, ROTI provides information on large scale length of ionospheric irregularities which is related to the Nyquist period and components of the ionospheric projection of the satellite's motion and the irregularities in a direction perpendicular to the propagation path (Basu et al., 1999). For observation data of 30-s interval, the Nyquist period is 60s. If the vector sum of these two velocities is, normally, 100 m/s in the equatorial region, then the irregularity scale length sampled by 30-s ROT and 30s-5 min ROTI corresponds to 6 km. Similarly, the irregularity scale length sampled by 1-s ROT and 1s-1 min ROTI corresponds to 200m. A more detailed relationship between the irregularities scale and drift velocity as well as receiver sampling rates is illustrated in Figure 2 in Mrak et al. (2021), one can refer there for a

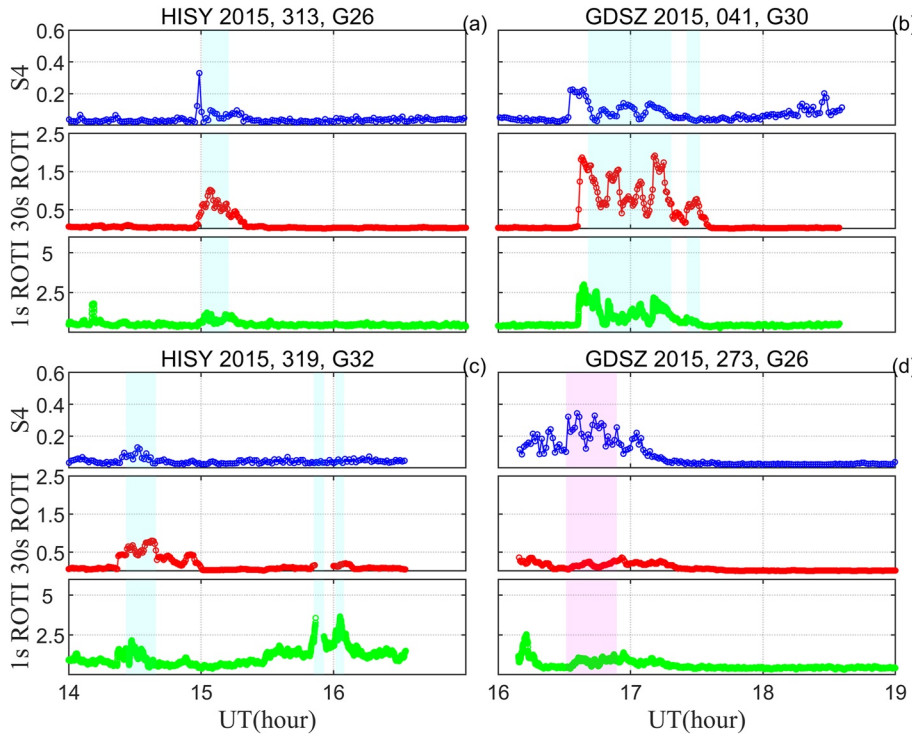

Figure 8. Time series of S_4, 30s-5 min ROTI and 1s-1 min ROTI (in TECU/minutes unit) for G26 on DOY 313, G32 on DOY 319 in 2015 at HISY (left column) and for G30 on DOY 041, G26 on DOY 273 in 2015 at GDSZ (right column).

more intuitive vision. The coexistence attribute of multi-scales of irregularities in the ionosphere enables the ISM with ROTI, while, the inconsistency of their quantity might degrade the performance of ISM with ROTI. Two cases were chosen from HISY and GDSZ respectively to show the deviation between ROTI and S_4.

Figure 8 exhibits the time series of S_4, 30s-5 min ROTI, and 1s-1 min ROTI for satellites G26 on DOY 313, satellite G32 on 319 in 2015 at HISY; satellite G30 on DOY 041, satellite G26 on DOY 273 in 2015 at GDSZ, respectively. The significant inconsistencies between ROTI and S_4 are highlighted in the shadow area in the figure. As is shown in subfigure (a), the series of 30s-5 min ROTI in the shadow area indicate the existence of ionospheric irregularities during 15:00–15:20 UT. However, the series of corresponding S_4 and 1s-1 min ROTI in the same period suggest no ionospheric scintillation/irregularities occurs during the same period. The essential reason for this situation is that ionospheric irregularities at scales > Fresnel scale causing ROTI but not S_4. A similar situation is also found in the shadow area of subfigure (b) and first shadow area in subfigure (c). Similarly, the latter two shadow areas in subfigure (c) suggest the existence of irregularities measured by 1s-1 min ROTI while S_4 and 30s-5 min ROTI keep quiet. In addition, in the magenta shadow area in the subfigure (d), the S_4 suggests the occurrence of ionospheric scintillation during 16 and 17 UT but both 30s-5 min ROTI and 1s-1 min ROTI do not reveal ionospheric irregularities. In such case, ROTI will underreport the ionospheric scintillation. Both deviations between ROTI and S_4 are mainly due to that ROTI is measuring different "band" of irregularities that scintillation index S_4 measures. When directly relating ROTI to ionospheric scintillation, we have to consider its reliability. Here we deem the situation when S_4 is smaller than its critical value of scintillation (0.2) but ROTI is larger than its critical value of scintillation at the same epoch as misreporting of ionospheric scintillation by ROTI and vice is deemed as underreporting of ionospheric scintillation by ROTI. In order to evaluate the impact of the deviation between ROTI and S_4 on the performance of ROTI in indicating the occurrence of ionospheric scintillation, the accuracy of different ROTI in reporting ionospheric scintillation is compared. The rate of misreporting/underreporting of ionospheric scintillation is defined as the ratio of the amount of misreported/underreported scintillation by ROTI to the amount of reported scintillation by S_4. In addition to these two cases, the rest is the rate of the accurate report which can be regarded as the reliability of ROTI in indicating the occurrence of scintillation. The statistics of the rates of misreporting, underreporting, and accurate reporting of ionospheric scintillation by ROTI at HISY and GDSZ are shown in Figure 9. It can be seen that both 1s-1 min ROTI and 30s-5 min

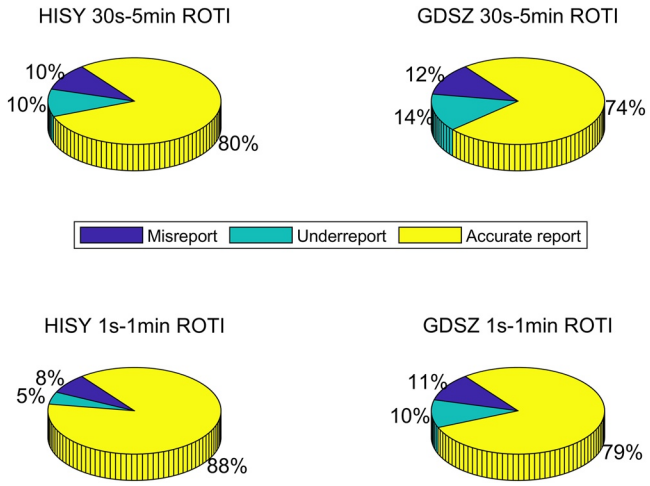

Figure 9. Statistics of the rates of misreport, underreport and accuracy of ionospheric scintillation monitored by Rate of change of Total electron content Index at HISY (left column) and GDSZ (right column).

ROTI have errors in reporting ionospheric scintillation but 1s-1 min ROTI is more accurate than 30s-5 min ROTI in reporting ionospheric scintillation. The reason that the rate of accurate report of ionospheric scintillation by ROTI obtained at HISY station is higher than that at GDSZ station may be due to the fact that the distance between ISM receiver and geodetic receiver at HISY (5 km) is closer than that at GDSZ (26 km) station. Therefore, the accuracy report obtained at HISY is more representative.

We define the event when a satellite's ROTI deviates from its S_4 (according to their own critical value of scintillation/irregularities) and lasts for more than 10 min as an event of deviation. In order to understand the impact of this kind of deviation on the reliability of ROTI in reflecting ionospheric scintillation, the correlation between ROTI and S_4 is calculated for each satellite and is classified according to whether the deviation event exists or not. The statistical results of the percentage of correlation between S_4 and ROTI are shown in Figure 10. The red color in the figure represents the existence of deviation and the blue color represents the non-existence of deviation. As shown by the result at GDSZ (right column in the figure), for 30s-5 min ROTI and S4, 60% of the correlations are between 0.55 ~ 0.75 and 65% of the correlations are between 0.75 ~ 0.9 according to their deviations exist or not; for 1s-1 min ROTI and S4 at GDSZ, 85% of the correlations are between 0.55–0.80 and 87% of the correlations are between 0.75 ~ 0.95 according to their deviations exist or not. As shown by the result at HISY (left column in the figure), for 30s-5 min ROTI and S_4, 60% of the correlations are between 0.45 ~ 0.7 and 60% of the correlations are between 0.65 ~ 0.85 according to their deviations exist or not; for 1s-1 min ROTI and S_4, 66% of the correlations are between 0.6 ~ 0.8 and 82% of the correlations are between 0.75 ~ 0.95 according to their deviations exist or not.

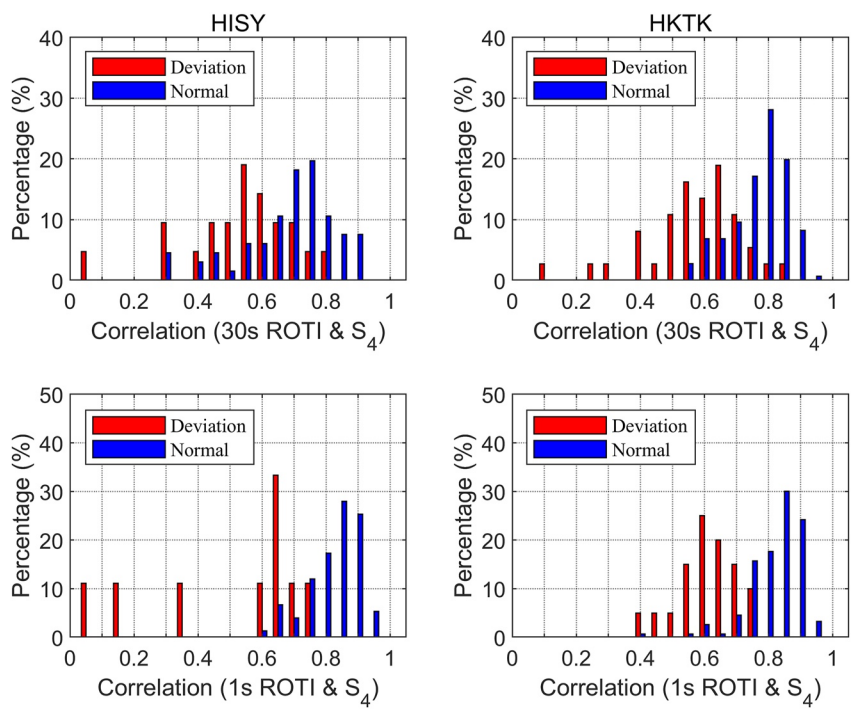

Figure 10. Percentage of correlation between Rate of change of Total electron content Index (ROTI) (30s-5 min ROTI and 1s-1 min ROTI) and S_4. The red color represents that deviation exists between ROTI and S_4; the blue color represents that deviation does not exist between ROTI and S_4.

4. Conclusions

Based on GPS observation data obtained from geodetic receivers and ISM receivers at HISY and GDSZ/HKTK station in year 2015, this work summarized the limitations of ROTI derived from common geodetic receivers in representing ionospheric scintillation and comprehensively evaluated the performance of ROTI in indicating the occurrence of ionospheric scintillation by comparing ROTI and amplitude scintillation index S_4.

The correlation between ROTI and amplitude scintillation index S_4 is found to be dependent on the satellite elevation angle where ionospheric scintillation occurs. The correlation between ROTI and S_4 increases linearly with the increase of elevation angle until the maximum elevation angle. This implies that ROTI has a weak performance in representing ionospheric scintillation at a low satellite elevation angle.

Large ionospheric variations between epochs of 30-s sampling interval data would cause erroneous reporting of cycle slips when a traditional threshold of cycle slip detection is adopted in the calculation of ROTI. Frequent cycle slips plus erroneous cycle slips interrupt the continuity of ROTI and reduce the integrity of ROTI during strong scintillation. The integrity of 30s-5 min ROTI determined by a traditional threshold of cycle slip detection is about 60% during ionospheric scintillation, implying 40% information of ionospheric scintillation is missed by 30s-5 min ROTI. We proved that the traditional threshold of cycle slip detection is constrained and proposed a more reasonable threshold of 0.25 m for 30-s sampling interval data. The integrity of 30s-5 min ROTI determined by the proposed threshold of cycle slip detection improved by 10%–15% compared with that determined by traditional threshold. Benefiting from the high sampling rate of 1-s sampling interval observation data as well as short calculation time interval, the integrity of 1s-1 min ROTI is about 90% during ionospheric scintillation.

The deviation of ROTI from S_4, which is probably induced by the difference of scale length of ionospheric irregularities monitored by S_4 and ROTI, limits the reliability of ROTI in indicating ionospheric scintillation and decreases the correlation between ROTI and S_4. Under the influence of the deviation between ROTI and S_4, the accuracy of 30s-5 min ROTI in reporting ionospheric scintillation could reach 80%, the accuracy of 1s-1 min ROTI in reporting ionospheric scintillation could reach 88%. At GDSZ, the deviations of 30s-5 min ROTI from S_4 at cause 60% of the correlations between them drop by 0.15 ∼ 0.2; the deviations of 1s-1 min ROTI from S_4 cause 85% of the correlations between them drop by 0.15 ∼ 0.2. At HISY, the deviations of 30s-5 min ROTI from S_4 cause 60% of the correlations between them drop by 0.15 ∼ 0.2; the deviations of 1s-1 min ROTI from S_4 cause 66% of the correlations between them drop by 0.15. In general, 1s-1 min ROTI gets a better performance in indicating the occurrence of ionospheric scintillation than 30s-5 min ROTI.

Data Availability Statement

The ionospheric TEC/scintillation data from GDSZ (Shenzhen) station can be downloaded via Data Center for Meridian Space Weather Monitoring Project (https://data2.meridianproject.ac.cn/data) after registration. The ionospheric scintillation data from Sanya (HISY) station can be downloaded after registration at https://gnss.shao.ac.cn/. The GPS observation data from HKTK station can be downloaded via Hong Kong Satellite Positioning Reference Station Network (https://www.geodetic.gov.hk/en/rinex/downv.aspx) or (ftp://ftp.geodetic.gov.hk/rinex3/). The GPS observation data from HISY station are available from the National Earthquake Infrastructure Service of China after registration approval via email at (cmonoc@seis.ac.cn).

Acknowledgments
This work was supported in part by National Natural Science Foundation of China (Grant No. 41730109, 12073063), in part by project ZR2021QD080 supported by Shandong Provincial Natural Science Foundation and State Key Laboratory of Geo-Information Engineering, No. SKLGIE2020-M-1-1. Wei Li thanks the constructive guidance and advice from researcher Maorong Ge at DasHelmholz-Zentrum Potsdam -Deutsches GeoForschungsZentrum, GFZ, Germany. Wei Li thanks the help from Professor Yin Fan at Wuhan University, and the help from Chunjiang Ma at University of national defense science and technology. The authors acknowledge the Chinese Meridian Project for providing ionospheric scintillation data. Acknowledgement for the data support from "China Earthquake Networks Center, National Earthquake Data Center (http://data.earthquake.cn)." Acknowledgment for the Lands Department of the Government of Hong Kong Special Administrative Region (HKSAR) for providing the GPS/GNSS data from the "Hong Kong Satellite Positioning Reference Station Network (SatRef) (https://www.geodetic.gov.hk/en/rinex/downv.aspx) or (ftp://ftp.geodetic.gov.hk/rinex3/)." Acknowledgement for the support from iGMAS (international GNSS Monitoring & Assessment System) and Shanghai Key Laboratory of Space Navigation and Positioning Techniques.

References

Aarons, J., Whitney, H. E., & Allen, R. S. (1975). Global morphology of ionospheric scintillations. *Proceedings of the IEEE*, *59*(2), 159–172. https://doi.org/10.1109/proc.1971.8122

Basu, S., Basu, S., Aarons, J., McClure, J. P., & Cousins, M. D. (1978). On the coexistence of kilometer- and meter-scale irregularities in the nighttime equatorial F region. *Journal of Geophysical Research. Part A: Space Physics*, *83*(A9), 4219–4226. https://doi.org/10.1029/JA083iA09p04219

Basu, S., Quinn, J., Doherty, P., & Quinn, J. M. (1999). A comparison of TEC fluctuations and scintillations at Ascension Island. *Journal of Atmospheric and Solar-Terrestrial Physics*, *61*(16), 1219–1226. https://doi.org/10.1016/s1364-6826(99)00052-8

Beach, T. L., & Kintner, P. M. (1999). Simultaneous Global Positioning System observations of equatorial scintillations and total electron content fluctuations. *Journal of Geophysical Research*, *104*(A10), 22553–22565. https://doi.org/10.1029/1999ja900220

Cai, C., Liu, Z., Xia, P., & Dai, W. (2013). Cycle slip detection and repair for undifferenced GPS observations under high ionospheric activity. *GPS Solutions*, *17*(2), 247–260. https://doi.org/10.1007/s10291-012-0275-7

Carrano, C. S., Groves, K. M., & Rino, C. L. (2019). On the relationship between the rate of Change of Total Electron Content Index (ROTI), Irregularity Strength (CkL), and the Scintillation Index (S4). *Journal of Geophysical Research: Space Physics*, *124*(3), 2099–2112. https://doi.org/10.1029/2018ja026353

Chen, D., Ye, S., Zhou, W., Zhou, W., Liu, Y., Jiang, P., et al. (2016). A double-differenced cycle slip detection and repair method for GNSS CORS network(Article). *GPS Solutions*, *20*(3), 439–450. https://doi.org/10.1007/s10291-015-0452-6

Chen, W., Gao, S., Hu, C., & Ding, C. X. (2008). *Effects of ionospheric disturbances on GPS observation in low latitude area*. GPS Solutions.

Cherniak, I., Krankowski, A., & Zakharenkova, I. (2014). Observation of the ionospheric irregularities over the Northern Hemisphere: Methodology and service. *Radio Science*, *49*(8), 653–662. https://doi.org/10.1002/2014rs005433

Cherniak, I., Krankowski, A., & Zakharenkova, I. (2018). ROTI maps: A new IGS ionospheric product characterizing the ionospheric irregularities occurrence. *GPS Solutions*, *22*(3), 1. https://doi.org/10.1007/s10291-018-0730-1

Cherniak, I., & Zakharenkova, I. (2015). Dependence of the high-latitude plasma irregularities on the auroral activity indices: A case study of 17 March 2015 geomagnetic storm. *Earth Planets and Space*, *67*(1), 151. https://doi.org/10.1186/s40623-015-0316-x

Cherniak, I., Zakharenkova, I., & Krankowski, A. (2014). Approaches for modeling ionosphere irregularities based on the TEC rate index. *Earth Planets and Space*, *66*(1), 165. https://doi.org/10.1186/s40623-014-0165-z

Conker, R. S., El-Arini, M. B., Hegarty, C. J., & Hsiao, T. (2003). Modeling the effects of ionospheric scintillation on GPS/satellite-based augmentation system availability. *Radio Science*, *38*, 1–23. https://doi.org/10.1029/2000rs002604

Doherty, P., Delay, S. H., Valladares, C. E., & Klobuchar, J. A. (2003). Ionospheric scintillation effects on GPS in the equatorial and auroral regions. *Annual of Navigation*, *50*(4), 235–245. https://doi.org/10.1002/j.2161-4296.2003.tb00332.x

Humphreys, T. E., Psiaki, M. L., & Kintner, P. M. (2010). Modeling the effects of ionospheric scintillation on GPS carrier phase tracking. *IEEE Transactions on Aerospace and Electronic Systems*, *46*(4), 1624–1637. https://doi.org/10.1109/taes.2010.5595583

Humphreys, T. E., Psiaki, M. L., Ledvina, B. M., Cerruti, A. P., & Kintner, P. M. (2010). Data-driven testbed for evaluating GPS carrier tracking loops in ionospheric scintillation. Aerospace and electronic systems. *IEEE Transactions on Aerospace and Electronic Systems*, *46*(4), 1609–1623. https://doi.org/10.1109/taes.2010.5595582

Jacobsen, K. S. (2014). The impact of different sampling rates and calculation time intervals on ROTI values. *Journal of Space Weather and Space Climate*, *4*, A33. https://doi.org/10.1051/swsc/2014031

Lee, C. C., Liu, J. Y., Reinisch, B. W., Chen, W. S., & Chu, F. D. (2005). The effects of the pre-reversal ExB drift, the EIA asymmetry, and magnetic activity on the equatorial spread F during solar maximum. *Annales Geophysicae*, *23*(3), 745–751. https://doi.org/10.5194/angeo-23-745-2005

Li, G., Ning, B., & Hong, Y. (2007). Analysis of ionospheric scintillation spectra and TEC in the Chinese low latitude region. *Earth Planets and Space*, *59*(4), 279–285. https://doi.org/10.1186/bf03353105

Liu, Z. (2011). A new automated cycle slip detection and repair method for a single dual-frequency GPS receiver. *Journal of Geodesy*, *85*(3), 171–183. https://doi.org/10.1007/s00190-010-0426-y

Ma, G., & Maruyama, T. (2006). A super bubble detected by dense GPS network at east Asian longitudes. *Geophysical Research Letters*, *33*(21), 241–255. https://doi.org/10.1029/2006gl027512

Mrak, S., Semeter, J., Nishimura, T., Coster, A. J., & Groves, K. (2021). Space weather at mid-latitudes: Leveraging geodetic GPS receivers for ionospheric scintillation science. In *Proceedings of the 34th international technical meeting of the satellite division of the institute of navigation (ION GNSS+ 2021)* (pp. 3910–3919).

Mrak, S., Semeter, J., Nishimura, Y., Rodrigues, F. S., Coster, A. J., & Groves, K. (2020). Leveraging geodetic GPS receivers for ionospheric scintillation science. *Radio Science*, *55*(11), e2020RS007131. https://doi.org/10.1029/2020rs007131

Muella, M., Paula, E., Kantor, I. J., Batista, I. S., Sobral, J., Abdu, M. A., et al. (2008). GPS L-band scintillations and ionospheric irregularity zonal drifts inferred at equatorial and low-latitude regions. *Journal of Atmospheric and Solar-Terrestrial Physics*, *70*(10), 1261–1272. https://doi.org/10.1016/j.jastp.2008.03.013

Pi, X., Iijima, B. A., & Lu, W. (2017). Effects of ionospheric scintillation on GNSS-based positioning. *Navigation*, *64*(1), 3–22. https://doi.org/10.1002/navi.182

Pi, X., Mannucci, A. J., Lindqwister, U. J., & Ho, C. M. (1997). Monitoring of global ionospheric irregularities using the worldwide GPS network. *Geophysical Research Letters*, *24*(18), 2283–2286. https://doi.org/10.1029/97gl02273

Pi, X., Mannucci, A. J., Valant-Spaight, B. L., Bar-Sever, Y. E., Romans, L. J., Skone, S., et al. (2013). *Observations of global and regional ionospheric irregularities and scintillation using GNSS tracking networks*.

Prikryl, P., Jayachandran, P. T., Mushini, S. C., Pokhotelov, D., MacDougall, J. W., Donovan, E., et al. (2010). GPS TEC, scintillation and cycle slips observed at high latitudes during solar minimum. *Annales Geophysicae*, *28*(6), 1307–1316. https://doi.org/10.5194/angeo-28-1307-2010

Tanna, H. J., Karia, S. P., & Pathak, K. N. (2013). A study of L band scintillations during the initial phase of rising solar activity at an Indian low latitude station. *Advances in Space Research*, *52*(3), 412–421. https://doi.org/10.1016/j.asr.2013.03.022

Thomas, R. M., Cervera, M. A., Eftaxiadis, K., Manurung, S. L., Saroso, S., Effendy, R. A. G., et al. (2001). A regional GPS receiver network for monitoring equatorial scintillation and total electron content. *Radio Science*, *36*(6), 1545–1557. https://doi.org/10.1029/2000rs002521

Wei, W., Li, W., Song, S., & Shao, L. (2019). *Study on the calculation strategies of ionospheric scintillation index ROTI from GPS*.

Woodman, R. F., & Hoz, C. L. (1976). Radar observations of F region equatorial irregularities. *Journal of Geophysical Research. Part A: Space Physics*, *81*(31), 5447–5466. https://doi.org/10.1029/JA081i031p05447

Xiong, C., Stolle, C., & Lhr, H. (2016). The swarm satellite loss of GPS signal and its relation to ionospheric plasma irregularities. *Space Weather-The International Journal of Research and Applications*, *14*(8), 563–577. https://doi.org/10.1002/2016sw001439

Xu, J., Zhu, J., & Li, L. (2007). Effects of a major storm on GPS amplitude scintillations and phase fluctuations at Wuhan in China. *Advances in Space Research*, *39*(8), 1318–1324. https://doi.org/10.1016/j.asr.2007.03.004

Yang, Z., & Liu, Z. (2015). Correlation between ROTI and Ionospheric Scintillation Indices using Hong Kong low-latitude GPS data. *GPS Solutions*, *20*(4), 815–824. https://doi.org/10.1007/s10291-015-0492-y

Yang, Z., & Morton, Y. T. J. (2020). Low-latitude GNSS ionospheric scintillation dependence on magnetic field orientation and impacts on positioning. *Journal of Geodesy*, *94*(6), 59. https://doi.org/10.1007/s00190-020-01391-7

Yang, Z., Mrak, S., & Morton, Y. (2020). Geomagnetic storm induced mid-latitude ionospheric plasma irregularities and their implications for GPS positioning over North America: A case study. In *2020 IEEE/ION position, location and navigation symposium (PLANS)*.

Zakharenkova, I., Astafyeva, E., & Cherniak, I. (2016). GPS and GLONASS observations of large-scale traveling ionospheric disturbances during the 2015 St. Patrick's Day storm. *Journal of Geophysical Research: Space Physics*, *121*, 12–156. https://doi.org/10.1002/2016ja023332

Zakharenkova, I. C., Krankowski, I., & Krankowski, A. (2019). Features of storm-induced ionospheric irregularities from ground-based and spaceborne GPS observations during the 2015 St. Patrick's Day storm. *Journal of Geophysical Research: Space Physics*, *124*(12), 10728–10748. https://doi.org/10.1029/2019ja026782

Zhang, D. H., Xiao, Z., Feng, M., Hao, Y. Q., Shi, L. Q., Yang, G. L., & Suo, Y. C. (2010). *Temporal dependence of GPS cycle slip related to ionospheric irregularities over China low-latitude region* (Vol. 8). Space Weather-the International Journal of Research & Applications.

Zhang, X., Guo, F., & Zhou, P. (2014). Improved precise point positioning in the presence of ionospheric scintillation. *GPS Solutions*, *18*(1), 51–60. https://doi.org/10.1007/s10291-012-0309-1

Zhang, X., Qi, Z., Jun, H., & Chao, K. (2017). *Improving TurboEdit real-time cycle slip detection by the construction of threshold model* (Vol. 42, pp. 285–292). Geomatics and Information Science of Wuhan University. https://doi.org/10.13203/j.whugis20150045